AGU PUBLICATIONS

Geophysical Research Letters

RESEARCH LETTER
10.1002/2014GL062301

Key Points:
- A new method is developed to analyze moisture budget parameters from satellites
- Organized system and isolated cumulus regimes differ in how they are maintained
- The mechanisms are illustrated based on a thermodynamic budget consideration

Correspondence to:
H. Masunaga,
masunaga@hyarc.nagoya-u.ac.jp

Citation:
Masunaga, H. (2014), Free-tropospheric moisture convergence and tropical convective regimes, *Geophys. Res. Lett.*, *41*, 8611–8618, doi:10.1002/2014GL062301.

Received 22 OCT 2014
Accepted 11 NOV 2014
Accepted article online 15 NOV 2014
Published online 1 DEC 2014

Free-tropospheric moisture convergence and tropical convective regimes

Hirohiko Masunaga[1]

[1] Hydrospheric Atmospheric Research Center, Nagoya University, Nagoya, Japan

Abstract This work searches for the key elements separating the dynamic and quiescent phases characterizing the tropical atmosphere. The analysis is performed with satellite measurements that are composited into statistical time series individually for the isolated cumulus and organized system regimes. Free-tropospheric (FT) moisture convergence, cloud-base (CB) moisture updraft, and FT precipitation efficiency (FTPE) are then derived under large-scale moisture budget constraints. Precipitation is fed primarily by FT moisture convergence while FTPE and CB moisture updraft amplify in tandem as organized systems develop. In the isolated cumulus regime, FT moisture remains weakly diverging over time accompanying little change of FTPE. A thermodynamic budget consideration suggests that organized systems develop under a self-sustaining growth of large-scale updraft in the dynamic phase, while the quiescent phase is maintained by stable, shallow circulation accompanying isolated cumuli.

1. Introduction

Tropical moist convection is constituted of a broad spectrum of cloud types ranging from shallow cumuli to deep convective and stratiform clouds. In a climatological picture widely accepted, shallow cumuli prevail under the descending branch of the Hadley circulation while clouds can develop deep into cumulonimbi within the ascending Hadley cell [*Simpson*, 1992; *Johnson et al.*, 1999]. This picture, however, does not necessarily provide a complete illustration to explain the regional and temporal variability of tropical convection. The occurrence of precipitating shallow cumuli is insensitive to large-scale vertical motion across the tropics although predominant over the central and east Pacific owing to the relative infrequency of deeper convection there [*Masunaga and Kummerow*, 2006]. Shallow cumulus clouds are therefore not specific to the regions with subsidence but are ubiquitous under the ascending branch of large-scale overturning circulations as well. Indeed, quiescent periods with no cold-topped clouds are more frequently observed than dynamic periods characterized by extensive deep convection even over the west Pacific warm pool [*Serra et al.*, 1997], which is an area considered from the climatological perspectives to harbor vigorous deep convection. Alternating occurrences of convectively active and suppressed phases have been extensively studied in the context of Madden-Julian Oscillation [*Madden and Julian*, 1972] and convectively coupled equatorial waves [*Kiladis et al.*, 2009]. It has been much less documented, however, what factors in the large-scale environment are crucial in general beyond the wave dynamics for separating the quiescent and dynamic phases over tropical oceans. This study is an attempt to isolate out the processes instrumental in a stable maintenance of the isolated cumulus regime and a self-sustaining growth in the organized system regime, by exploring observational evidence obtained from a suite of satellite instruments.

2. Data and Method

2.1. Satellite Data

Air temperature and water vapor soundings are obtained from the Aqua Atmospheric Infrared Sounder and Advanced Microwave Sounder Unit (AIRS/AMSU, hereafter AIRS collectively). The Aqua Advanced Microwave Scanning Radiometer for Earth Observing System (AMSR-E) provides surface precipitation, and radiative heating rate is obtained from the combined CloudSat and Cloud-Aerosol Lidar and Infrared Pathfinder Satellite Observation (CALIPSO) product. Although not explicitly discussed in this paper, other A-Train data sets and Quick Scatterometer (QuikSCAT) measurements are also incorporated in the composite analysis described below. Precipitating clouds detected by the Tropical Rainfall Measuring Mission (TRMM) Precipitation Radar (PR) define the base point in composite time series. The global tropical oceans bound between

15°S and 15°N are analyzed for 7 years from 1 December 2002 to 30 November 2009 with the exception of CloudSat data that are available only for the period from 1 July 2006 onward.

2.2. Composite Time Series of Moisture Budget Parameters

Key parameters to be analyzed in this work are derived under the moisture budget constraint imposed by the satellite measurements in the procedure briefly summarized below. Satellite soundings collected over a period of time are projected onto the composite time axis before and after the moment when the TRMM detects precipitating clouds [*Masunaga*, 2012]. A large sample of such soundings averaged for each time bin would constitute a continuous time series of the atmospheric variability associated with the occurrence of moist convection. The large-scale mean thermodynamic field is calculated from the cloud-cleared AIRS soundings blended with a semi-analytical estimate of in-cloud sounding. Moisture convergence is then diagnosed from the vertically integrated moisture budget equation, given the rest of the equation being constrained with the observations. The subcloud layer (SC) convergence is directly computed with QuikSCAT winds, leaving free-tropospheric (FT) moisture convergence and the vertical moisture flux at cloud base (CB) each isolated out as a budget residual. A complete description of the methodology is found in *Masunaga* [2013].

The population density of TRMM-detected convection, or the number count of raining PR pixels within the surrounding one-square-degree domain, is termed hereafter as the TRMM precipitation coverage. The composite time series are separately constructed depending on the TRMM precipitation coverage in order to differentiate a range of convective types. Following the definitions of *Masunaga* [2013], isolated cumulus clouds and highly organized systems are each extracted for TRMM precipitation coverages smaller than 25% and larger than 50%, respectively, to separately examine the two contrasting regimes of tropical convection, hereafter denoted as the *isolated cumulus regime* and the *organized system regime*. These convective regimes are analyzed as a proxy of the dynamic and quiescent phases.

2.3. Moisture Updraft and Downdraft at Cloud Base

An analysis method is next developed to evaluate the moisture updraft and downdraft at CB. The underlying concept is similar to the traditional approaches based on in situ sounding array data [e.g., *Yanai et al.*, 1973; *Johnson*, 1976]. The current approach is new in that it exploits satellite observations only, although the estimates are limited to CB instead of full vertical profiles.

The large-scale mean vertical moisture flux at CB, $\overline{qM_{CB}}$, is broken down into the updraft and downdraft components as

$$\overline{qM_{CB}} = q^*_{CB\text{-}} M^{\uparrow}_{CB} + q^a_{CB+} M^{\downarrow}_{CB} \tag{1}$$

where $q^*_{CB\text{-}}$ and q^a_{CB+} denote the saturation mixing ratio defined immediately below CB and the ambient vapor mixing ratio above CB, respectively, and $M^{\uparrow}_{CB}$ and $M^{\downarrow}_{CB}$ are the updraft and downdraft mass fluxes at CB. The formulation would be more accurate if the moisture downdraft term in equation (1) was split into saturated and unsaturated components, but these two components are very difficult to individually identify in the observations currently available. Those terms may be safely combined when the difference in vapor mixing ratio between the saturated and unsaturated downdrafts is negligible. This assumption is not entirely groundless because, although a saturated downdraft has a higher relative humidity by definition than the surrounding unsaturated air, this difference would be mitigated by a temperature difference due to a stronger evaporative cooling in the saturated downdraft than its environment. The current treatment of the downdraft terms is nevertheless incomplete, and we will focus mainly on the updraft in the remainder of this paper.

Equation (1) is merged with the mass conservation at CB, $\overline{M_{CB}} = M^{\uparrow}_{CB} + M^{\downarrow}_{CB}$, to yield the updraft and downdraft mass fluxes as

$$M^{\uparrow}_{CB} = \frac{\overline{qM_{CB}} - q^a_{CB+}\overline{M_{CB}}}{q^*_{CB\text{-}} - q^a_{CB+}} \tag{2}$$

$$M^{\downarrow}_{CB} = -\frac{\overline{qM_{CB}} - q^*_{CB\text{-}}\overline{M_{CB}}}{q^*_{CB\text{-}} - q^a_{CB+}} \tag{3}$$

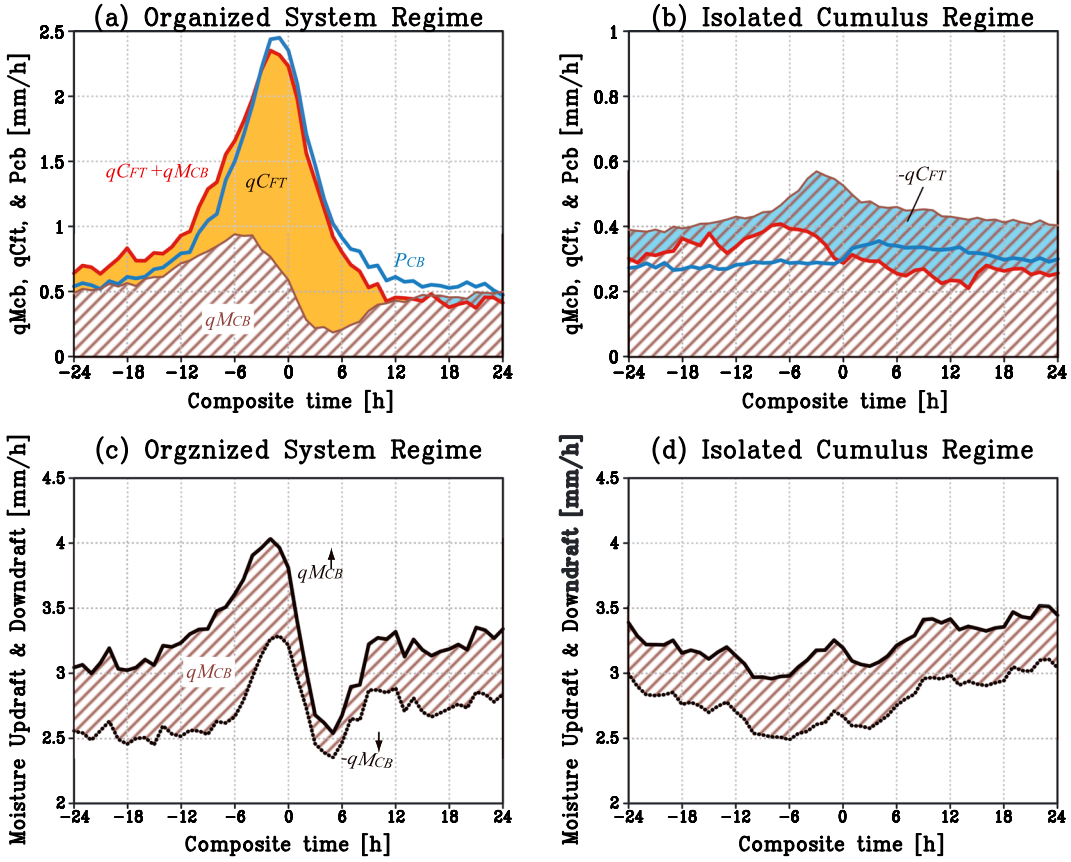

Figure 1. Composite time series of different moisture budget parameters (mm h^{-1}) for (a) the organized system regime and (b) the isolated cumulus regime. FT moisture convergence ($\overline{qC_{FT}}$, shaded in yellow where positive and in light blue where negative) is plotted on the top of net vertical moisture flux at CB ($\overline{qM_{CB}}$, hatched). The sum of these two quantities are highlighted in red. (c and d) As Figures 1a and 1b but for CB moisture updraft ($qM^{\uparrow}_{CB}$, solid) and CB moisture downdraft with the sign flipped ($-qM^{\downarrow}_{CB}$, dotted), where the domain bound between the two curves is equal to $\overline{qM_{CB}}$ (hatched) by definition.

Each variable on the right-hand side of equations (2) and (3) are known from the observations (e.g., equations (25) and (31) of *Masunaga* [2013] for $\overline{qM_{CB}}$ and $\overline{M_{CB}}$, respectively).

Precipitation at CB, required to constrain the FT moisture budget, is given by adding the reevaporation rate within the SC to the observed surface precipitation. The SC reevaporation is estimated so that evaporative cooling balances out the SC heat budget under the assumption that the vertical eddy flux of dry static energy (DSE) vanishes at CB, using equations (26) and (29) of *Masunaga* [2013]. The vertical eddy DSE flux is thermodynamically unlikely to stay negative since otherwise heat would be transported downward against buoyancy, so the SC reevaporation derived this way provides its upper limit under the given constraint. The estimated reevaporation rate is found to vary between 1% and 10% of surface precipitation rate.

3. Results

An overall illustration of the temporal variation in the FT moisture budget is first presented for each isolated cumulus and organized system regime. Figure 1 shows the temporal variability, for ±24 h about the time of TRMM-detected convection, in the large-scale mean moisture budget equation integrated over FT,

$$\partial_t \overline{q}_{FT} = \overline{qC}_{FT} + \overline{qM}_{CB} - \overline{P}_{CB}, \tag{4}$$

where overbar denotes the spatial average over a large-scale domain or a circular area with the radius of 100 km, $\partial_t q_{FT}$ is FT moisture storage, qC_{FT} is FT moisture convergence, and P_{CB} is precipitation at CB.

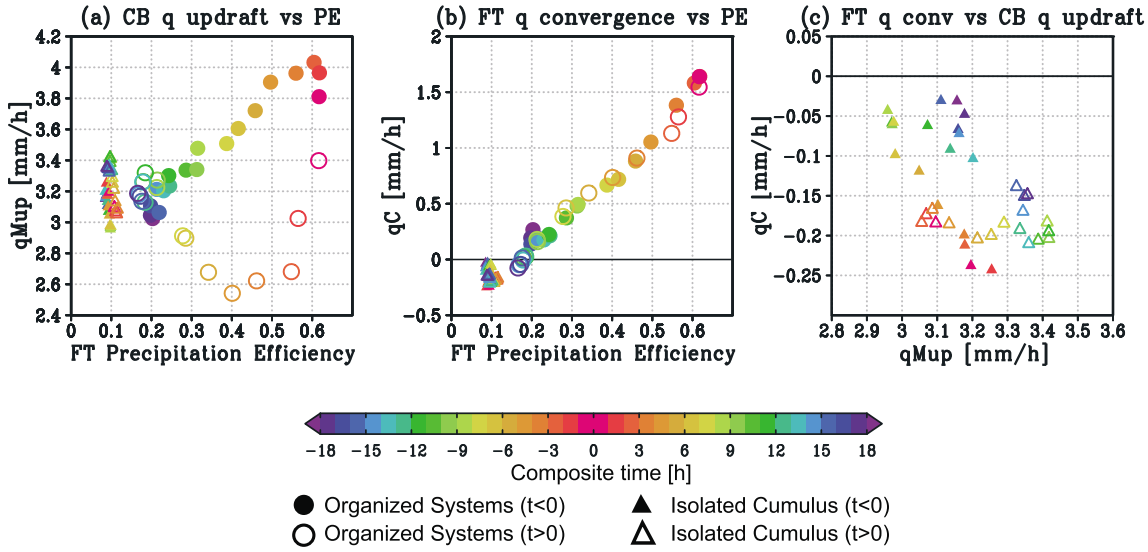

Figure 2. The evolutionary trajectory projected onto the plane of (a) CB moisture updraft (ordinate) and FTPE (abscissa), (b) FT moisture convergence (ordinate) and FTPE (abscissa), and (c) FT moisture convergence (ordinate) and CB moisture updraft (abscissa). Color indicates time with filled marks for $t < 0$ and open marks otherwise. The organized system regime and isolated cumulus regime are designated by circles and triangles, respectively. Only the isolated cumulus regime is shown in Figure 2c.

Note that $\overline{qC}_{FT}$ nominally includes horizontal moisture advection in the formulation above although the advection term is small in any case at spatial scales of current interest. The sum of $\overline{qC}_{FT}$ and $\overline{qM}_{CB}$ (red curve in Figure 1) roughly amounts to precipitation except for a minor disagreement that corresponds to moisture storage.

In the organized system regime (Figure 1a), precipitation is initially fed mostly by CB moisture flux, while FT moisture convergence takes an increasing share of moisture supply as precipitation evolves toward its peak. FT convergence remains a dominant source of moisture during several hours after the peak. Since a majority of convective precipitation likely originates from SC water vapor, a substantial fraction of FT moisture convergence presumably experiences a mesoscale downdraft into SC before condensed out in the convective updraft. It is found from Figure 1c that the contribution of FT convergence is small to the total moisture carried by each updraft and downdraft at CB, because CB moisture updraft and downdraft are individually much larger than FT moisture convergence or than any other variables plotted in Figure 1a. The proportion of how much moisture within the updraft air is to be precipitated out will be later discussed in terms of precipitation efficiency. Precipitation in the isolated cumulus regime undergoes only a slight increase at time zero, preceded by a modest enhancement of CB moisture flux (Figure 1b) although its updraft and downdraft components hardly show a systematic variability over time (Figure 1d). FT moisture stays weakly diverging throughout the evolution, implying that in this regime precipitation is not fed with FT moisture. Recalling that the current study area is limited to tropical latitudes (15°S–15°N), one should not confuse the "FT" divergence with whole-tropospheric moisture divergence known to dominate the subtropical climatology. Rather, SC moisture is converging even in the isolated cumulus regime barely strongly enough to overcome the FT divergence when integrated over the entire troposphere as will be seen in section 4.

The contrasting behaviors in the two convective regimes are next examined in terms of CB moisture updraft, $q^*_{CB\text{-}}M^{\uparrow}_{CB}$, and *FT precipitation efficiency* (FTPE) defined as $\overline{P}_{CB}/(q^*_{CB\text{-}}M^{\uparrow}_{CB})$, which may be considered as a variant of conventional large-scale precipitation efficiency with the FT and SC contributions separately defined [*Sui et al.*, 2007, and references therein]. FTPE, when plotted together with CB moisture updraft, would provide an insight into different aspects of convective characteristics as illustrated below. The current definition of FTPE does not explicitly include FT moisture convergence as a moisture input. As mentioned above, CB moisture updraft virtually contains the FT-originating moisture that is eventually converted into convective rainfall, so that the denominator in the definition of FTPE implicitly includes to a large extent the contribution of FT moisture convergence to precipitation.

Figure 2a shows the evolutionary trajectory in the plane of CB moisture updraft and FTPE. The organized system regime (filled circles) experiences a steady increase in both moisture updraft and FTPE until a few hours before time zero when precipitation reaches its maximum (Figure 1a). Moisture updraft then sharply drops to a minimum before it mildly rises back to the initial level while FTPE monotonically decreases (open circles). The returning track is quite distinct from the first half of the trajectory, presumably because stratiform precipitation, dominating late stages in the life cycle of organized convective systems, does not accompany as robust an updraft in the lower troposphere as deep convection typical of the earlier stages. Isolated cumulus clouds (triangles) do not exhibit any discernible fluctuation in FTPE around 0.1 while experiencing a modest variation of moisture updraft. This infers that in the isolated cumulus regime shallow cumuli vary over time only in population, being accompanied by some variation in CB moisture updraft, without growing much into vigorous convection as implied by a constant FTPE. This makes a remarkable contrast to the organized system regime, where FTPE changes drastically between 0.2 and 0.6, indicative of a significant modulation in the nature of convective clouds during the evolution.

We have seen in Figure 1 that the two convective regimes are especially distinct from each other in the behavior of FT moisture convergence. Figure 2b illustrates the evolution of FT moisture convergence as a function of FTPE. In the organized system regime, FT moisture convergence and FTPE evolve in tandem, tightly coupled together onto a linear trajectory throughout the entire period. FT moisture convergence stays negative and hardly variable in the isolated cumulus regime (Figure 2b) as was evident in Figure 1b. FT moisture convergence is plotted against CB moisture updraft for the isolated cumulus regime in Figure 2c, where a weak negative correlation, if any correlation at all, emerges between these two quantities. It follows that, on the contrary to the organized system regime, the FT moisture divergence may slightly strengthen at times when isolated cumuli increase in number, possibly working against, rather than promoting, a further deepening of cumuli.

4. Discussion and Conclusion

The motivation of this work is to seek the aspects of large-scale thermodynamics that differentiate tropical convective regimes in search for the potential factors separating the convectively quiescent and dynamic phases. To this end, a composite time series of the FT moisture budget variability is constructed from a combination of various satellite measurements. Main conclusions are outlined as follows. FT moisture convergence provides a dominant moisture source feeding precipitation during the peak in the organized system regime, while the isolated cumulus regime is accompanied at any time by a weak moisture divergence in FT. The fact that FT moisture convergence differs even in sign suggests that these two convective regimes may be driven by essentially different mechanisms in terms of the FT moisture budget.

Masunaga and L'Ecuyer [2014] investigated the processes underlying moist convection and its environment in the organized system regime on the basis of large-scale vertical velocity derived from the same data set as currently analyzed. They found that the gross moist stability (GMS) [*Neelin and Held*, 1987] is bound tightly to zero while precipitation intensifies to its peak, inferring a mechanics that (marginally) allows the self-sustaining development of convection and large-scale vertical motion [*Raymond et al.*, 2009]. The vertical mode decomposition technique devised by *Masunaga and L'Ecuyer* [2014] is applied here to briefly look into the dynamics behind the observed behaviors in each convective regime. Figures 3a and 3b show the mode decomposition of FT moisture convergence into the first and second baroclinic modes and the shallow mode combined with the time-independent background component. The first baroclinic mode predominantly accounts for FT moisture convergence in the organized system regime (Figure 3a), while in the isolated cumulus regime it is the shallow mode, or a thin layer of modest updraft immediately above CB, that dominates the entire evolution with the first baroclinic mode being minimal throughout (Figure 3b). This clearly delineates the contrast in FT dynamics between the two regimes: the organized system regime is driven by lower to middle tropospheric convergence that efficiently provides FT with moisture, while FT moisture is diverged away immediately above CB by a shallow overturning circulation. Figures 3c and 3d presents the whole-tropospheric (WT) moisture convergence (as energy flux, $\overline{LqC_{\mathrm{WT}}}$) and WT moist static energy (MSE) convergence ($\overline{hC_{\mathrm{WT}}}$) with WT radiative heating rate ($\overline{Q_{R,\mathrm{WT}}}$) plotted on its top. These three terms together constitute a version of GMS that is defined as $-(\overline{hC_{\mathrm{WT}}} + \overline{Q_{R,\mathrm{WT}}})/\overline{LqC_{\mathrm{WT}}}$. In the organized system regime, moisture convergence (rescaled as labeled on right) greatly overwhelms MSE divergence and radiative heating in magnitude during active convection (Figure 3c), indicative of zero GMS as noted above. SC moisture convergence more than cancels out FT moisture divergence in the isolated cumulus regime when

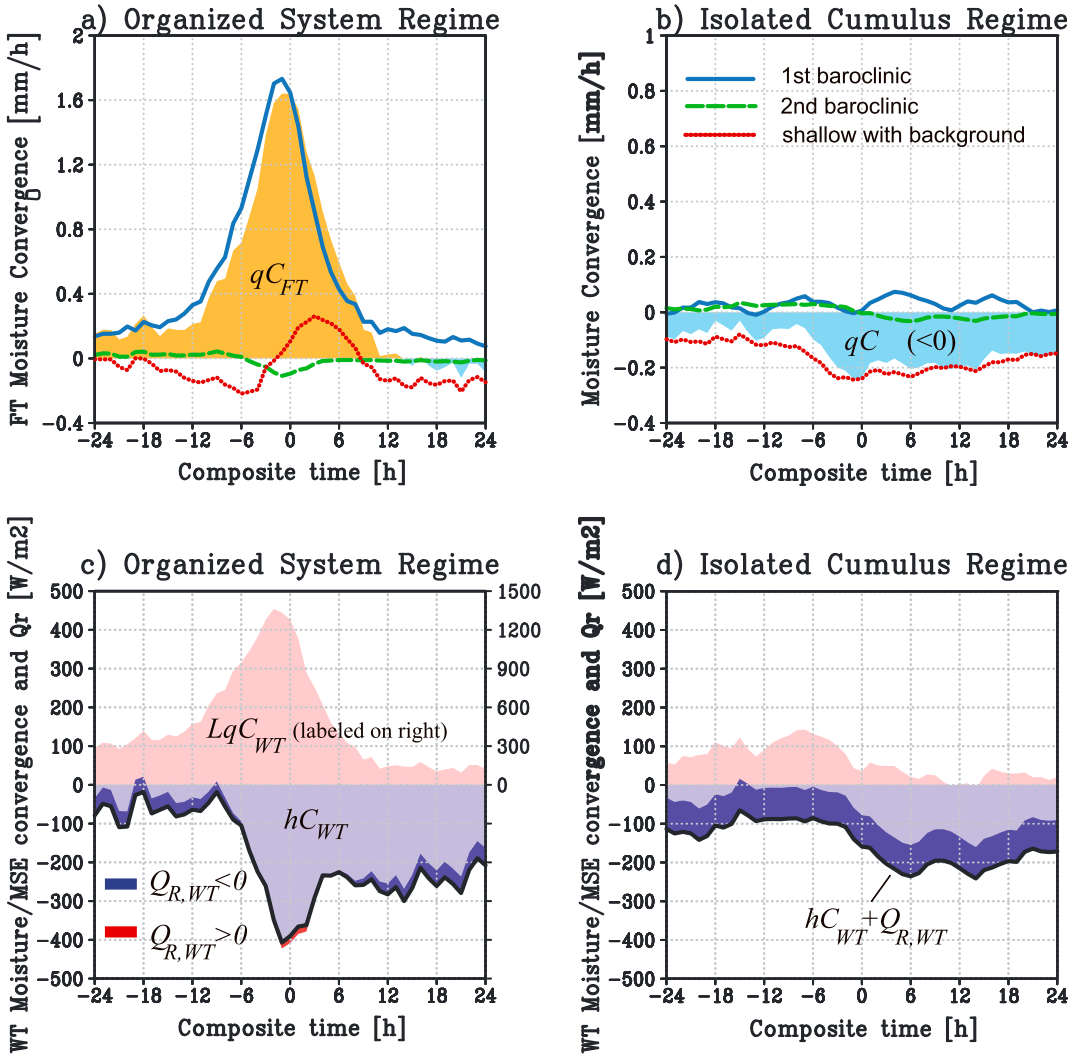

Figure 3. Composite time series of FT moisture convergence ($\overline{qC_{FT}}$) (mm h^{-1}) and its vertical mode decomposition for (a) the organized system regime and (b) the isolated cumulus regime. The first baroclinic mode (blue solid), second baroclinic mode (green dashed), and shallow mode with the background profile (red dotted) are plotted together with their total (shaded in yellow where positive and in blue where negative). The first baroclinic mode is labeled on the right axis in Figure 3a. (c and d) As Figures 3a and 3b but for WT moisture convergence ($\overline{LqC_{WT}}$, shaded in light red), WT MSE convergence ($\overline{hC_{WT}}$, shaded in light purple), and WT radiative heating rate ($\overline{Q_{R,WT}}$, shaded in dark purple where negative and in dark red where positive). Radiative heating rate is drawn on the top of MSE convergence so they together delineate their sum ($\overline{hC_{WT}} + \overline{Q_{R,WT}}$, black solid).

integrated together into WT moisture convergence, which is nevertheless not so large in magnitude that it consistently dominates the sum of MSE divergence and radiative cooling (Figure 3d). The isolated cumulus regime has a larger radiative cooling than the organized system regime presumably owing to a smaller coverage of high clouds. GMS therefore stays positive, suggesting a stable regulation of the isolated cumulus regime. It is noted that MSE is diverging in the isolated cumulus regime despite the absence of the first baroclinic mode, seemingly contradicting the expectation that shallow circulation imports moisture and MSE [e.g., *Back and Bretherton*, 2006]. The MSE divergence here arises from a weak upper tropospheric ascent prevailing in the background that exports more MSE than imported by the shallow mode. The background field is a critical element in the vertical mode decomposition of a tropical sounding conducted by *Masunaga and L'Ecuyer* [2014]. Possible origins of the background weak ascent are left to be explored.

Figure 4 presents a schematic summary illustrating the contrasting roles of FT moisture convergence between the two convective regimes. Figure 4a shows the organized system regime in its developing phase,

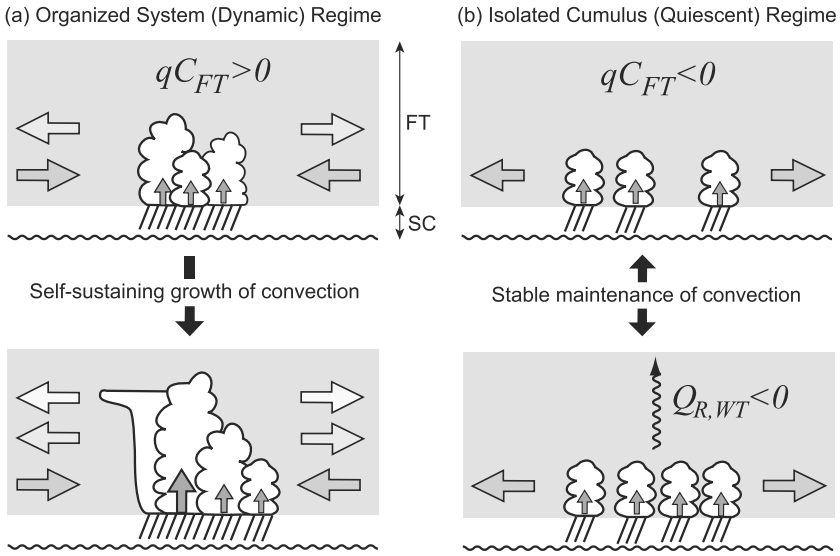

Figure 4. Schematic to illustrate the proposed hypothesis (see text). The free troposphere is designated by a light gray box. Horizontal arrows indicate large-scale mean moisture flow (shaded darker where more humid), and vertical arrows represent CB moisture updraft.

where large-scale dynamics consist of lower tropospheric convergence and upper tropospheric divergence brought by the first baroclinic mode. The lower tropospheric convergence supplies moisture just enough to fuel large-scale updraft through the depth of the troposphere with the help of eddy moisture transport due to penetrating convective clouds [*Masunaga and L'Ecuyer*, 2014]. The tight coupling observed between FT moisture convergence and FTPE suggests a close collaboration between large-scale dynamics and moist convection. A thermodynamic consideration with moisture and MSE convergences suggests that the organized system regime involves a self-sustaining growth of convection and large-scale updraft, giving rise to a dynamic phase. In the isolated cumulus regime (Figure 4b), the shallow mode is prevalent throughout and provides a weak but consistent FT moisture divergence. Isolated cumuli vary only in population without developing into a vigorous convective system in this regime. Persistently positive GMS as well as the observed correlation between FT moisture divergence and CB moisture updraft favors the speculation that the isolated cumulus regime is stably maintained without the ability to grow by itself, which presumably accounts for the longevity of a quiescent phase.

FT moisture divergence could often occur in the eastern Pacific intertropical convergence zone (ITCZ), where the meridional circulation is climatologically shallow [*Zhang et al.*, 2004]. The eastern Pacific ITCZ, however, is highly variable in that the dynamics phase associated with unstable environmental soundings is no less typical than the quiescent phase [*Raymond et al.*, 2003]. A shallow overturning circulation indeed appears across different tropical areas as a secondary mode to the deep Hadley cells [*Trenberth et al.*, 2000; *Zhang et al.*, 2008]. As such, the quiescent and dynamic phases coexist widely over tropical oceans, suggesting that a transition between the phases commonly occurs. The present findings appear to suggest that a quiescent phase could be destabilized into a dynamic phase once MSE divergence is counteracted by an import of MSE, for any reasons including the effect of radiative cooling reduction, to the extent that it enables a self-sustaining growth of deep convection and circulation. *Raymond et al.* [2006] highlighted surface heat fluxes as a key element that destabilizes a quiescent phase to a dynamic phase. Further investigations need to be done to narrow down the specific factors that are responsible for the transition.

Acknowledgments
The author is grateful to Yousuke Sato, Dave Raymond, and the anonymous reviewer for their helpful comments. The AIRS/AMSU product was provided by Goddard Earth Sciences (GES) Data and Information Services Center (DISC) (disc.sci.gsfc.nasa.gov), the TRMM PR (2A25) data set by the Japan Aerospace Exploration Agency (JAXA), the GPROF 2010 precipitation product by Colorado State University (rain.atmos.colostate.edu/RAINMAP10), the AMSR-E SST and CWV product by Remote Sensing Systems (www.remss.com), the CloudSat 2B-CLDCLASS and 2B-FLXHR-LIDAR data sets by the CloudSat Data Processing Center (www.cloudsat.cira.colostate.edu), and QuikSCAT SeaWinds ocean wind vector data by the Physical Oceanography Distributed Active Archive Center (PO.DAAC) at the NASA Jet Propulsion Laboratory (podaac.jpl.nasa.gov). This work is supported by the Japan Society for the Promotion of Science (JSPS) Grant-in-Aid for Challenging Exploratory Research (26610150) and by JAXA (JX-PSPC-399837).

The Editor thanks David Raymond and an anonymous reviewer for their assistance in evaluating this paper.

References

Back, L. E., and C. S. Bretherton (2006), Geographic variability in the export of moist static energy and vertical motion profiles in the tropical Pacific, *Geophys. Res. Lett.*, *33*, L17810, doi:10.1029/2006GL026672.

Johnson, R. H. (1976), Role of convective-scale precipitation downdrafts in cumulus and synoptic-scale interactions, *J. Atmos. Sci.*, *33*, 1890–1910.

Johnson, R. H., T. M. Rickenbach, S. A. Rutledge, P. E. Ciesielski, and W. H. Schubert (1999), Trimodal characteristics of tropical convection, *J. Clim.*, *12*, 2397–2418.

Kiladis, G. N., M. C. Wheeler, P. T. Haertel, K. H. Straub, and P. E. Roundy (2009), Convectively coupled equatorial waves, *Rev. Geophys.*, *47*, RG2003, doi:10.1029/2008RG000266.

Madden, R. A., and P. R. Julian (1972), Description of global-scale circulation cells in the tropics with a 40-50 day period, *J. Atmos. Sci.*, *29*, 1109–1123.

Masunaga, H. (2012), A satellite study of the atmospheric forcing and response to moist convection over tropical and subtropical oceans, *J. Atmos. Sci.*, *69*, 150–167.

Masunaga, H. (2013), A satellite study of tropical moist convection and environmental variability: A moisture and thermal budget analysis, *J. Atmos. Sci.*, *70*, 2443–2466.

Masunaga, H., and C. D. Kummerow (2006), Observations of tropical precipitating clouds ranging from shallow to deep convective systems, *Geophys. Res. Lett.*, *33*, L16805, doi:10.1029/2006GL026547.

Masunaga, H., and T. S. L'Ecuyer (2014), A mechanism of tropical convection inferred from observed variability in the moist static energy budget, *J. Atmos. Sci.*, *71*, 3747–3766.

Neelin, J. D., and I. M. Held (1987), Modeling tropical convergence based on the moist static energy budget, *Mon. Weather Rev.*, *115*, 3–12.

Raymond, D. J., G. B. Raga, C. S. Bretherton, J. Molinari, C. López-Carrillo, and Ž. Fuchs (2003), Convective forcing in the intertropical convergence zone of the eastern Pacific, *J. Atmos. Sci.*, *60*, 2064–2082.

Raymond, D. J., C. S. Bretherton, and J. Molinari (2006), Dynamics of the intertropical convergence zone of the east Pacific, *J. Atmos. Sci.*, *63*, 582–597.

Raymond, D. J., S. L. Sessions, A. H. Sobel, and Ž. Fuchs (2009), The mechanics of gross moist stability, *J. Adv. Model. Earth Syst.*, *1*, 9, doi:10.3894/JAMES.2009.1.9.

Serra, Y. L., D. P. Rogers, D. E. Hagan, C. A. Friehe, R. L. Grossman, R. A. Weller, and S. Anderson (1997), Atmospheric boundary layer over the central and western equatorial Pacific Ocean observed during COARE and CEPEX, *J. Geophys. Res.*, *102*, 23,217–23,237.

Simpson, J. (1992), Global circulation and tropical cloud activity, in *The Global Role of Tropical Rainfall*, edited by J. S. Theon et al., pp. 77–92, A. Deepak Publishing, Hampton, Va.

Sui, C.-H., X. Li, and M.-J. Yang (2007), On the definition of precipitation efficiency, *J. Atmos. Sci.*, *64*, 4506–4513.

Trenberth, K. E., D. P. Stepaniak, and J. M. Caron (2000), The global monsoon as seen through the divergent atmospheric circulation, *J. Clim.*, *13*, 3969–3993.

Yanai, M., S. Esbensen, and J.-H. Chu (1973), Determination of bulk properties of tropical cloud clusters from large-scale heat and moisture budgets, *J. Atmos. Sci.*, *30*, 611–627.

Zhang, C., M. McGauley, and N. A. Bond (2004), Shallow meridional circulation in the tropical eastern Pacific, *J. Clim.*, *17*, 133–139.

Zhang, C., D. S. Nolan, C. D. Thorncroft, and H. Nguyen (2008), Shallow meridional circulations in the tropical atmosphere, *J. Clim.*, *21*, 3453–3470.